AlInAsSb/InGaAs single-photon avalanche diodes with high avalanche breakdown probability

Kubra Circir[1], Daniel Herrera[1], Jiayi Shao[2], Everett D. Fraser[2], Paul R. Pinsukanjana[2], and Joe C. Campbell[1,*]
[1]Department of Electrical and Computer Engineering, University of Virginia, Charlottesville, Virginia 22903, USA
[2]Intelligent Epitaxy Technology, Inc., 1250 E. Collins Blvd., Richardson, Texas 75081, USA
*jcc7s@virginia.edu

Abstract: A key characteristic of single-photon avalanche diodes (SPADs) is the photon detection efficiency (PDE), which can be expressed as PDE = $\eta \times P_{av}$, where η is the external quantum efficiency and P_{av} is the avalanche breakdown probability. InGaAs/InP SPADs are widely used for single-photon counting in the short-wavelength infrared. However, their PDE remains moderate because the InP multiplier has a relatively high *k* value (the ratio of the hole to electron ionization coefficients), which limits P_{av}. A high P_{av} is essential for achieving SPADs with near-unity PDE. The very low *k* values of Sb-based APDs enable higher P_{av} than InGaAs/InP SPADs. We report AlInAsSb/InGaAs SPADs on InP operating at 1550 nm, with P_{av} values greater than 90% at an over-bias of less than 6%.

Single-photon detection is important for a wide range of emerging technologies, including quantum communication,[1] quantum computing,[2] and LIDAR.[3] Single-photon detectors with high photon detection efficiency (PDE) and low dark count rate (DCR) are necessary for these applications, particularly at 1550 nm, where optical fiber losses are lowest. Superconducting nanowire single-photon detectors (SNSPDs) currently achieve PDEs greater than 90%, DCR less than 0.01 cps, and timing jitter in the picosecond range.[4] However, these detectors typically need to operate below 4 K, have a very small active area, and show polarization-dependent sensitivity. Single-photon avalanche diodes (SPADs) are an alternative because they can overcome these issues at higher temperatures.

For near-IR detection, InP-based SPADs employing InGaAs absorbers are widely adopted, especially for operation at 1550 nm. These devices are typically based on separate absorption, charge, and multiplication (SACM) structures to decouple photon absorption from avalanche multiplication. State-of-the-art InP/InGaAs devices have demonstrated DCR values as low as 1–10 Hz/μm² at temperatures near 225 K.[5–8] Their corresponding PDE values remain relatively modest, with the best reported values in the 40–60% range. This is because intrinsic properties of the InP multiplier fundamentally constrain these devices. In particular, a relatively high *k* value (~0.4[9]) of InP leads to less deterministic avalanche triggering, resulting in a more gradual avalanche breakdown probability, P_{av}. Therefore, practically attainable P_{av} restricts maximum PDE values, even though P_{av} can theoretically reach unity at very high excess bias. Recently, it has been shown that Sb-based multipliers achieve higher P_{av} at a given excess bias level due to their low *k* value.[10] Notably, simulations of AlAsSb multipliers, which have *k* values as low as ∼0.005,[11] indicate that P_{av} can exceed 80%, whereas P_{av} reach ∼51% for InP multipliers under the same over-bias.[10]

The quaternary $Al_xIn_{1-x}As_ySb_{1-y}$ (referred to by Al concentration as $Al_xInAsSb$) alloy has attracted interest due to its favorable material characteristics for both linear-mode APDs and Geiger-mode SPADs.

The epitaxial layers can be grown lattice-matched on GaSb or semi-insulating InP substrates. Based on the AlInAsSb material system grown on GaSb substrate, APDs with low dark current,[12,13] high gain,[14,15] extremely low noise[16,17] as well as SPADs with high P_{av}[18,19] have been demonstrated. More recently, $Al_{0.79}InAsSb$ multipliers grown lattice-matched on InP substrates have emerged as a promising alternative to conventional InGaAs/InP SACM devices. Linear-mode AlInAsSb/InGaAs APDs have been demonstrated with k values as low as ~ 0.04[20,21] and a low breakdown temperature coefficient, remaining below 6.7mV/K/μm.[20] Additionally, $Al_{0.79}InAsSb$ multipliers have been reported to achieve P_{av} values as high as 85% at room temperature for an over-bias of 8%.[22] However, single-photon characterization of AlInAsSb/InGaAs SPADs has not yet been explored. In this work, AlInAsSb/InGaAs SACM structure on InP was designed specifically for Geiger-mode operation, and single-photon characterization of these devices was performed at 1550 nm.

Fig. 1 shows the AlInAsSb/InGaAs separate absorption charge multiplication (SACM) epilayer structure grown by Molecular Beam Epitaxy (MBE) and lattice-matched to a semi-insulating InP substrate. The p-contact and blocking epi-stack provide an ohmic contact while establishing a diffusion barrier for electrons generated in the absorber. As the absorber, a slightly p-doped $In_{0.53}Ga_{0.47}As$ (hereafter InGaAs) has been included by converting its doping polarity from n- to p-type to prevent band-to-band tunneling. A previous study[12] demonstrates the effectiveness of a p-type absorber by comparing two SACM designs with and without p-type compensation. Bandgap grading between the charge and absorber layers is implemented in two distinct layers. In the first layer, the bandgap is stepped to half the charge bandgap. The following layer serves as an intermediate bandgap without grading all the way down to the absorber bandgap, which helps prevent high electric-field buildup in the narrow bandgap and reduces the dark current contribution from band-to-band tunneling. The doping concentration and thickness of the charge layer are intentionally adjusted to achieve punch-through near the breakdown voltage. This ensures that a sufficiently high electric field for impact ionization is established in the multiplication region before depletion extends into the absorber. Therefore, the absorber electric field remains lower than in typical linear-mode APD designs when the device breaks down, resulting in lower dark current. A thicker multiplier has been shown to increase avalanche breakdown probability at lower excess-bias levels in Sb-based APDs.[10] In a previous study, an SACM structure with a 1 μm-thick $Al_{0.79}InAsSb$ multiplier showed a higher breakdown probability than one with a thicker InP multiplier.[22] In this work, a 1 μm-thick $Al_{0.79}InAsSb$ multiplier is similarly inserted into the SACM structure for 1550 nm absorption. Finally, highly doped n-type contact layers are used to achieve better ohmic contact. Devices were patterned into circular mesas using standard photolithography and wet etching in a $C_6H_8O_7$:H_3PO_4:H_2O_2:H_2O acid solution. After mesa etching, Ti/Au contact metals were deposited by e-beam evaporation, and the mesa sidewalls were passivated with SU-8 polymer.

Fig. 2 shows the measured current-voltage (I-V) characteristics of a 150-μm-diameter SPAD device at 200 K under dark and illuminated conditions. Before breakdown, the dark current stabilizes at very low levels (~10^{-12}-10^{-13} A) and shows weak bias dependence. This suggests that tunneling and surface leakage currents do not dominate the current. The 2-step grading layer design eliminates the risk of tunneling without stepping all the way down to the absorber bandgap, and higher charge doping keeps the electric field low in the low-bandgap absorber. Furthermore, surface leakage current is greatly suppressed by keeping the electric field away from the mesa sidewalls due to bevelling from wet etching.

This results in a softer avalanche breakdown, confirming bulk-dominated breakdown behavior.

Since the structure is intentionally designed with higher charge doping, the device punches through near breakdown. This results in a noticeable gain at the punch-through voltage. In typical linear-mode APDs, the unity-gain point can be determined from the photocurrent, which remains nearly flat near the punch-through voltage. Since this SACM structure was designed for SPAD operation, it is difficult to determine the unity-gain point from the photocurrent. For such a device, there are two techniques for determining the unity external quantum efficiency (EQE). One approach is the gain simulation, which involves extracting the electric field in the multiplier by simulating the epilayer structure at each bias point. This was accomplished with the CHARGE solver in ANSYS Lumerical simulation software. Then, the electron and hole impact-ionization coefficients can be derived from this electric-field profile, and the gain is estimated at a specific bias assuming pure electron injection.[22] Comparison of the simulated gain of 15.9 at 65 V with the measured responsivity yielded a quantum efficiency of 55%. Another method is to use a control structure with the same epilayer parameters, except for charge doping. The charge doping is kept lower in the control structure to maintain a low electric field in the multiplier, resulting in unity gain at the punch-through voltage. Therefore, unity-EQE can be directly measured at the punch-through voltage. Here, the EQE was obtained by measuring the control device at the punch-through voltage, where the gain is unity. Fig. 3 shows the measured room-temperature unity-EQE for a 200-µm diameter device. In the EQE measurement, a commercially available strained InGaAs detector was used as a reference detector, and the wavelength was scanned from 500 nm to 1800 nm using a Newport monochromator. The measured unity-EQE at 1550 nm is ~55%, which is consistent with the gain simulation result.
K.

Single-photon characterization was performed using a Lakeshore cryogenic probe station cooled with liquid nitrogen and equipped with a gated-quenching circuit. This setup has been described in detail in previous work.[18] The DC bias was set below the breakdown voltage, while a 5-ns-wide gate pulse with 100-ps rise/fall times was applied above the breakdown voltage at a repetition rate of 10 kHz. For PDE measurements, the device was top-illuminated with 1550 nm light using a lensed fiber with a 2.5 µm spot size focused on the device center to ensure pure-electron injection into the multiplier. A picosecond pulsed diode laser was optically attenuated to 0.1 photons per pulse. The pulsed laser was synchronized with the voltage pulses to illuminate the device when it was over-biased. The count statistics were measured using a PicoQuant HydraHarp 400 counter. The discriminator level was set to the lowest possible value to eliminate counts caused by the circuit's capacitive transient. The integration time was set to 10 s.

Figure 4 shows the DCR-PDE relationship at 200 K. The unity-gain quantum efficiency serves as an upper limit for PDE, corresponding to an avalanche breakdown probability of 100%. A total of five devices were measured, and their DCR values were area-normalized because the devices were larger than state-of-the-art InP-based SPADs. The area-normalized DCR ranges from 0.01 to 1 kHz/µm², which is one order of magnitude lower than that of AlGaAsSb/InGaAs SPADs designed for linear-mode operation.[23] This suggests that a lower electric field in the absorber suppresses dark counts. The peak measured PDE values exceed 51%, approaching the unity-gain EQE limit, indicating a high P_{av} value.

To demonstrate the P_{av} curve over a wide range of over-bias voltages, devices were further overbiased, even though they already had PDE values close to unity-gain EQE. These measurements show smaller fluctuations around the highest PDE values but higher DCR due to larger over-bias, and are therefore included in Fig. 5 to demonstrate P_{av} saturation. These P_{av} values were calculated from PDE measurements using the relation Pav = PDE/η, where η is the unity-quantum efficiency. Fig. 5 shows measured average P_{av} values as a function of over-bias percentage for the $Al_{0.79}InAsSb/InGaAs$ SPADs at 200 K. The standard deviation of P_{av} was calculated at each over-bias percentage. The measured P_{av} curve is compared with its numerical simulation at the same temperature and with the previously reported SACM structure with $Al_{0.79}InAsSb$ multiplier/absorber layers.[22] Numerical simulation of P_{av} was performed using Lumerical's CHARGE solver to obtain the electric-field profiles from a two-dimensional cross-section of the structure over a range of applied biases. The electric field distribution through the multiplier was then used as input to Lumerical's "atp" script to compute the ionization integrals.[24] In the simulation, the breakdown voltage was determined as the voltage at which P_{av} becomes non-zero. The parameters for electron and hole ionization coefficients were obtained by curve fitting and inserted into the P_{av} simulation. $Al_{0.79}InAsSb$ ionization coefficients have been reported at room temperature in a previous work.[21] The temperature dependence of the ionization coefficients has been investigated in materials such as AlInAs[25] and $Al_{0.7}InAsSb$[26] using excess-noise measurements. In these works, it has been demonstrated that the hole ionization coefficient, β, decreases, while the electron ionization coefficient, α, slightly increases as temperature decreases. This relation results in a lower k value, leading P_{av} to have a stronger dependence on over-bias at lower temperatures. A previous study[19] has also experimentally demonstrated a stronger dependence of P_{av} on over-bias for the $Al_{0.7}InAsSb$ multiplier. Therefore, the ionization coefficients of $Al_{0.79}InAsSb$ at room temperature were scaled to 200 K using the same scale factor reported for the $Al_{0.7}InAsSb$ multiplier.

As shown in Fig. 5, a 1 μm-thick $Al_{0.79}InAsSb$ multiplier achieves an average P_{av} of 85% at an over-bias of 8.2% at 295 K. Incorporating the same multiplier into the InGaAs SACM structure increases dark current because of the lower-bandgap absorber. To enable single-photon characterization, the temperature was reduced to 200 K. The measured P_{av} shows a stronger dependence on over-bias, consistent with the simulation, owing to greater asymmetry in the ionization coefficients at the lower temperature. As a result, P_{av} rises more rapidly, yielding an average value approaching 95% at 200 K for over-bias levels below 6%. At higher over-bias levels, the standard deviation across devices remains below 3%.

In this work, we report $Al_{0.79}InAsSb/InGaAs$ SPADs on InP, specifically designed for Geiger-mode operation at 1550 nm. By integrating an Sb-based multiplier with an InGaAs absorber in the SACM structure, P_{av} values exceeding 90% were achieved at over-bias levels below 6%. This enables efficient transfer of linear-mode unity-gain EQE to Geiger-mode operation, yielding high PDE. Compared to state-of-the-art InP/InGaAs SPADs, the significantly lower k value of the $Al_{0.79}InAsSb$ multiplier enables much higher PDE, which is fundamentally limited by the higher k value of the InP multiplier. These III-V SPADs on an InP substrate can be heterogeneously integrated with waveguides to achieve quantum efficiency approaching unity.[27] Since $Al_{0.79}InAsSb$ multipliers exhibit higher P_{av}, these waveguide-coupled SPAD devices can pave the way toward near-unity PDE in integrated photonic circuits.

This work was supported by the National Science Foundation (2533557) and the National Science Foundation Grant OSI-2531569 [NQVL:QSTD:Design: Quantum Computing Applications of Photonics (QCAP)]

The authors have no conflicts to disclose.

The data that support the findings of this study are available from the corresponding author upon reasonable request.

References

1. E. Diamanti, H.-K. Lo, B. Qi, and Z. Yuan, Z. Npj Quantum Inf. **2**, 16025 (2016).
2. N. Maring, A. Fyrillas, M. Pont, E. Ivanov, P. Stepanov, N. Margaria, W. Hease, A. Pishchagin, A. Lemaitre, I. Sagnes, T. H. Au, S. Boissier, E. Bertasi, A. Baert, M. Valdivia, M. Billard, O. Acar, A.Rrieussel, R. Mezher, S. C. Wein, A. Salavrakos, P. Sinnott, D. A. Fioretto, P.-E. Emeriau, N. Belabas, S. Mansfield, Pl. Senellart, J. Senellart, and N. Somaschi, Nat. Photonics **18**, 603–609 (2024).
3. R. H. Hadfield, J. Leach, F. Fleming, D. J. Paul, C.-H. Tan, J. S. Ng, R. K. Henderson, and G. S. Buller, Optica **10**, 1124-1141 (2023).
4. L. You, Nanophotonics **9**, 2673–2692 (2020).
5. E. Kizilkan, U. Karaca, V. Pesic, M.-J. Lee, C. Bruschini, A. J. Springthorpe, A. W. Walker, C. Flueraru, O J. Pitts, and E. Charbon, IEEE J. Sel. Top. Quantum Electron. **28**, 1–9 (2022).
6. F. Signorelli, F. Telesca, E. Conca, F. A. Della, A. Ruggeri, A. Giudice, and A. Tosi, IEEE J. Sel. Top. Quantum Electron. **28**, 1–10 (2022).
7. Y.-Q. Fang, W. Chen, T.-H. Ao, C. Liu, W. Li, X.-J. Gao, J.Zhang, and J.-W. Pan, Rev. Sci. Instrum. **91**, 083102 (2020).
8. S. H. Baek, S.-C. Yang, C.-Y. Park, C.-W. Park, S.-B. Cho, and S.-W. Ryu, Korean Phys. Soc. **78**, 634–641 (2021).
9. F. Osaka and T. Mikawa, IEEE J. Quantum Electron. **22**, 471–478 (1986).
10. J. Ahmed, S. Xie, B. Liang, X. Yi, X. Jin, M. Kesaria, J. P. R. David, and D. L. Huffaker, IEEE J. Quantum Electron. **57**, 1–6 (2021).
11. X. Yi, S. Xie, B. Liang, L. W. Lim, J. S. Cheong, M. C. Debnath, D. L. Huffaker, C. H. Tan, and J. P. R. David, Nat. Photonics **13**, 683–686 (2019).
12. A. H. Jones, S.D. March, A. A. Dadey, A. J. Muhowski, S. R. Bank, and J. C. Campbell, IEEE J. Quantum Electron. **58**, 1–6 (2022).
13. J. A. McArthur, A. A. Dadey, K. Circir, H. Karimi, D. Wei, E. Y. Wang, J. C. Campbell, and S. R. Bank Appl. Phys. Lett. **126**, 261102 (2025).
14. A. A. Dadey, J. A. McArthur, A. Kamboj, S.R. Bank, D.Wasserman, and J. C. Campbell APL Photonics **8**, 036101 (2023).
15. D. Chen, S. D. March, A. H. Jones, Y. Shen, A. A. Dadey, K. Sun, J. A. McArthur, A.M. Skipper, X. Xue, B. Guo, J. Bai, S. R. Bank, and J. C. Campbell, Nat. Photonics **17**, 594–600 (2023).
16. A. H. Jones, S. D. March, S. R. Bank, and J. C. Campbell, Nat. Photonics **14**, 559–563 (2020).
17. A. A. Dadey, A. H. Jones, S. D. March, S. R. Bank, and J. C. Campbell Optica **10**, 1353-1357 (2023).

18. D. J. Herrera, A. A. Dadey, S. D. March, S. R. Bank, and J. C. Campbell Opt. Express **32**, 2106–2113 (2024).
19. D. J. Herrera, A. A. Dadey, K. Circir, J. Shao, E. D. Fraser, P. R. Pinsukanjana, and J. C. Campbell Appl. Phys. Lett. **127**, 153302 (2025).
20. B. Guo, M. Schwartz, S. H. Kodati, K. M. McNicholas, H. Jung, S. Lee, J. Konowitch, D. Chen, J. Bai, X. Guo, T. J. Ronningen, C. H. Grein, J. C. Campbell, and S. Krishna, APL Photonics **8**, 116112 (2023).
21. T. J. Ronningen, S. H. Kodati, X. Jin, S. Lee, H. Jung, X. Tao, H. I. J. Lewis, M. Schwartz, N. Gajowski, P. Martyniuk, B. Guo, A. H. Jones, J. C. Campbell, C. Grein, J. P. R. David, and S. Krishna, Appl. Phys. Lett. **123**, 131110 (2023).
22. D. Herrera, A. D. Dadey, K. Circir, J. Shao, E. D. Fraser, P. R. Pinsukanjana, and J. C. Campbell, J. Appl. Phys. **137**, 153102 (2025).
23. J. Taylor-Mew, X. Collins, B. White, C. H. Tan, and J. S. Ng, IEEE Trans. Electron Devices **71**, 1994–1998 (2024).
24. R. J. McIntyre, IEEE Trans. Electron Devices **20**, 637–641 (1973).
25. Y. Yuan, J. Zheng, Y. Tan, Y. Peng, A. K. Rockwell, S. R. Bank, A. W. Ghosh, and J. C. Campbell, Photonics Res. **6**, 794-799 (2018).
26. Y. Yuan, A. K. Rockwell, Y. Peng, J. Zheng, S. D. March, A. H. Jones, M. Ren, S. R. Bank, and J. C. Campbell, J. Light. Technol. **37**, 3647–3654 (2019).
27. T. Fatema, M. W. Xuan, P. Singaraju, T. Kim, K. Circir, X. Guo, D. J. Herrera, J. C. Campbell, M. Dagenais, and A. Beling, Opt. Express **34**, 8787-8794 (2026).

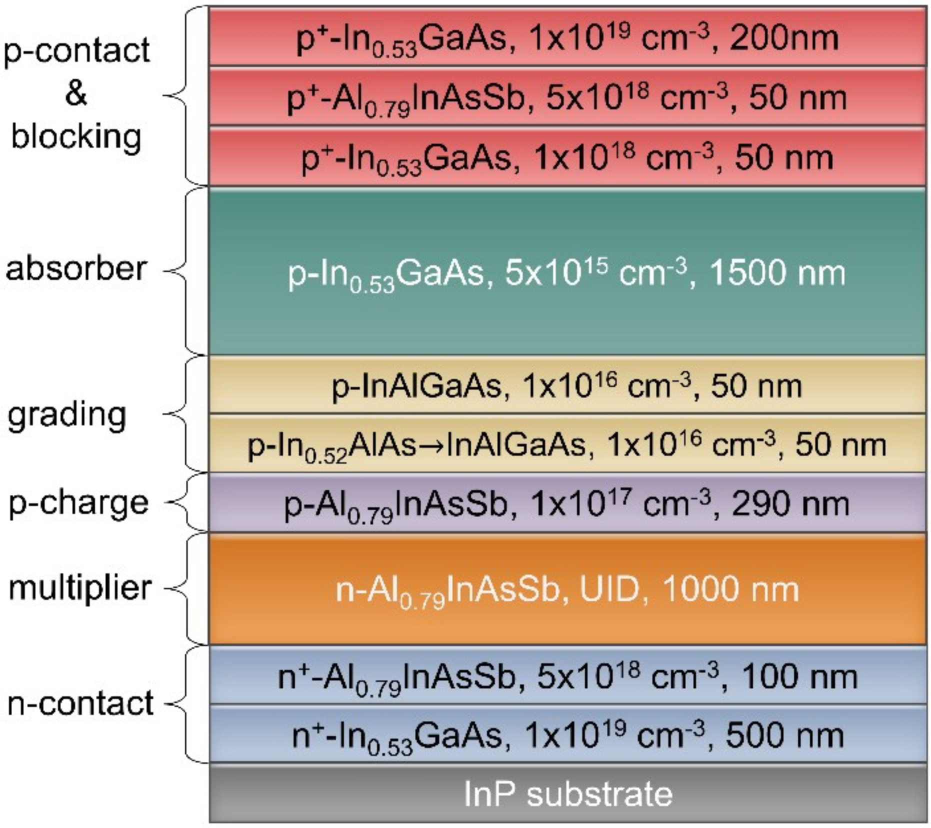

Fig. 1. Epitaxial layer structure of an $Al_{0.79}InAsSb$/InGaAs SACM SPAD on a semi-insulating InP substrate.

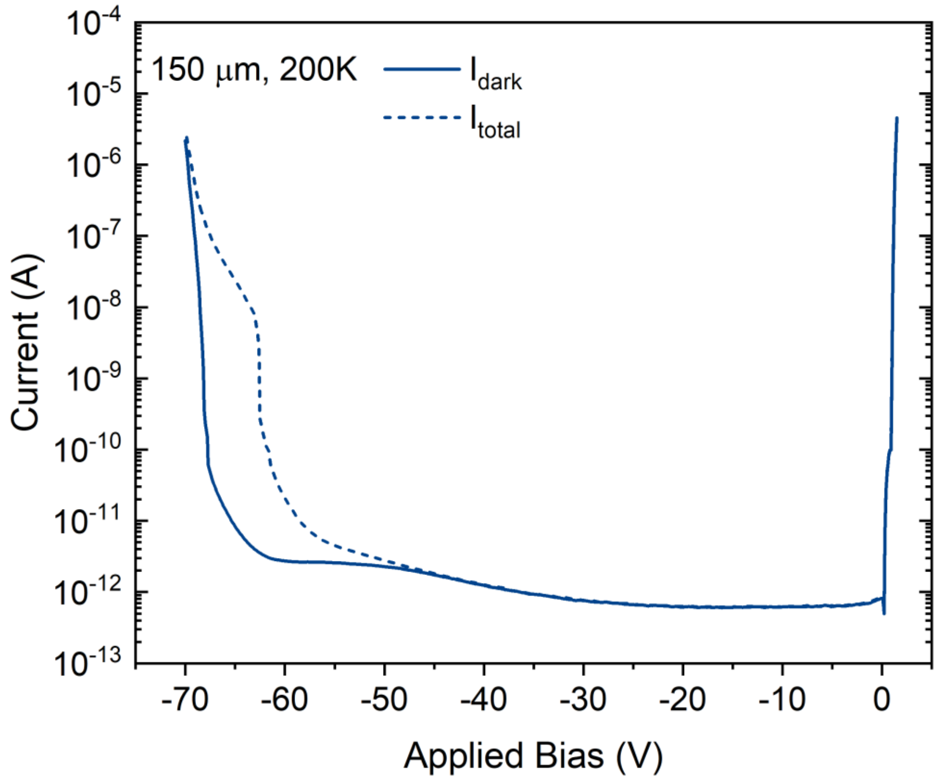

Fig. 2. Dark and 1550 nm illuminated I-V characteristics of a 150-μm diameter SACM device measured at 200

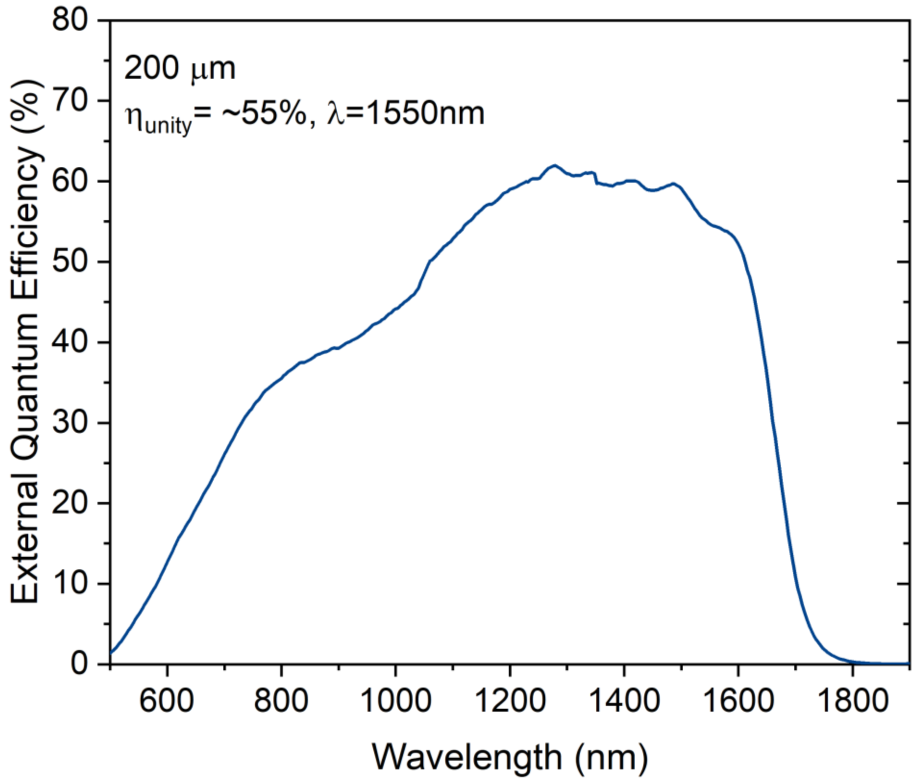

Fig. 3. Spectral unity-gain EQE between 500 nm and 1800 nm.

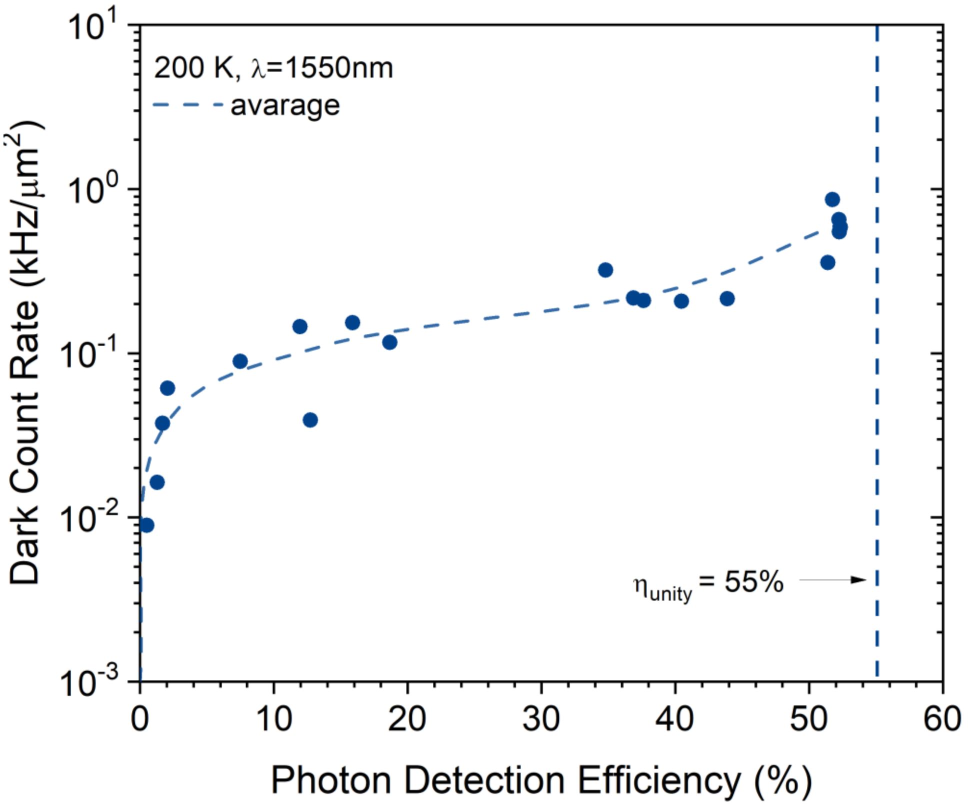

Fig. 4. DCR versus PDE measured for $Al_{0.79}InAsSb/InGaAs$ SACM SPADs at 200 K. The dashed curve and vertical dashed line indicate the average values and unity-gain EQE at 1550 nm, respectively.

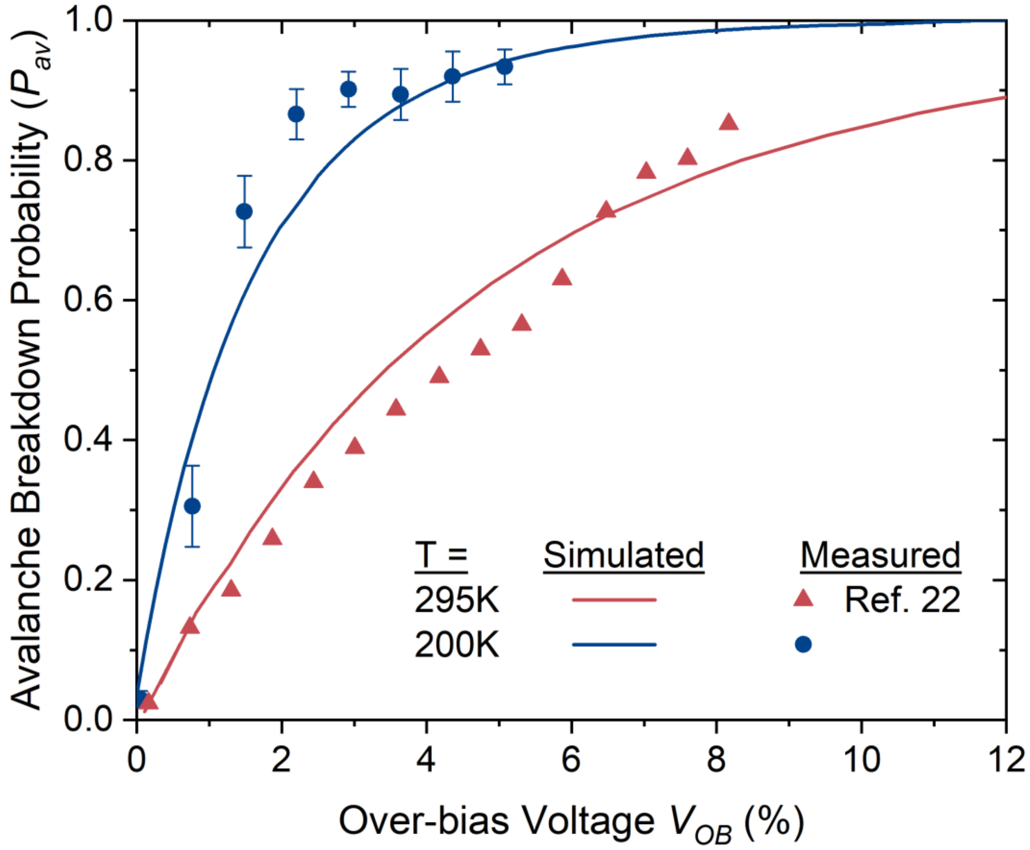

Fig. 5. Simulated and measured avalanche breakdown probability as a function of over-bias voltage for $Al_{0.79}InAsSb/InGaAs$ SACM at 200 K (blue) and $Al_{0.79}InAsSb$ SACM at 295 K (Red)[22].